Shap. Mem. Superelasticity (2017) 3:485–498
https://doi.org/10.1007/s40830-017-0133-0

TECHNICAL ARTICLE

The Measurement and Interpretation of Transformation Temperatures in Nitinol

T. W. Duerig[1] · A. R. Pelton[2] · K. Bhattacharya[3]

Published online: 6 November 2017

Abstract A previous paper (Duerig and Bhattacharya in Shap Mem Superelasticity 1:153–161, 2015) introduced several engineering considerations surrounding the R-phase in Nitinol and highlighted a common, if not pervasive, misconception regarding the use of the term A_f by the medical device industry. This paper brings additional data to bear on the issue and proposes more accurate terminology. Moreover, a variety of tools are used to establish the forward and reverse stress–temperature phase diagrams for a superelastic wire typical of that used in medical devices. Once established, the two most common methods of measuring transformation temperatures, Differential Scanning Calorimetry and Bend Free Recovery, are tested against the observed behavior. Light is also shed upon the origin of the Clausius–Clapeyron ratio ($d\sigma/dT$), the triple point, and why such large variations are reported in superelastic alloys.

Keywords Aging · Martensite · NiTi < Materials · Phase diagram · Superelasticity · R-phase

✉ T. W. Duerig
tom.duerig@nitinol.com

A. R. Pelton
alan.pelton@g-rau.com

K. Bhattacharya
bhatta@caltech.edu

[1] Nitinol Devices and Components, 47533 Westinghouse Dr., Fremont, CA 94539, USA

[2] G.RAU Inc., 3350 Scott Blvd. Bldg. 37B, Santa Clara, CA 95054, USA

[3] Division of Engineering and Applied Sciences, California Institute of Technology, Pasadena, CA 91125, USA

Introduction

The shape memory community often uses transformation temperature, and in particular the Austenite finish temperature (A_f), to predict and control the unloading stiffness of superelastic Nitinol, with the assumption that stabilizing Austenite (lowering transformation temperatures) results in higher plateau stresses. A previous paper [1] pointed out the fallacy of inferring plateau stresses from A_f except when the B19' Martensite phase (M) reverts directly to the B2 Austenite phase (A). While such direct transformation occurs in equiatomic and fully annealed Ni-rich alloys, it is rare in the superelastic conditions used for most medical devices. Superelastic medical devices generally require a high resistance to plastic deformation, obtained by introducing cold work and age hardening. Both of these hardening mechanisms create microstructural stress fields that hinder the advance of Martensite/Austenite phase boundaries. Suppressing M allows a competing martensitic phase to appear called the R-phase (R). Whilst the entropy of R is greater than M, the kinetic barriers to formation are substantially less, particularly in the presence of microstructural stress inhomogeneities.

Figure 1 introduces some of the objectives of this paper, by considering the differential scanning calorimetry (DSC) and tensile stress–strain responses of three different heat treatments of the same alloy [2]. Note that, one can obtain excellent superelastic properties at temperatures below A_f (red curve in Fig. 1). Moreover, even though the M_p temperature is sequentially suppressed from the black, blue, and red curves, no increase in the loading plateau is observed, i.e., while Martensite is increasingly difficult to thermally induce, the stress necessary to induce Martensite is not following the same trend. As will be shown, a full understanding of the competition between A, R, and M,

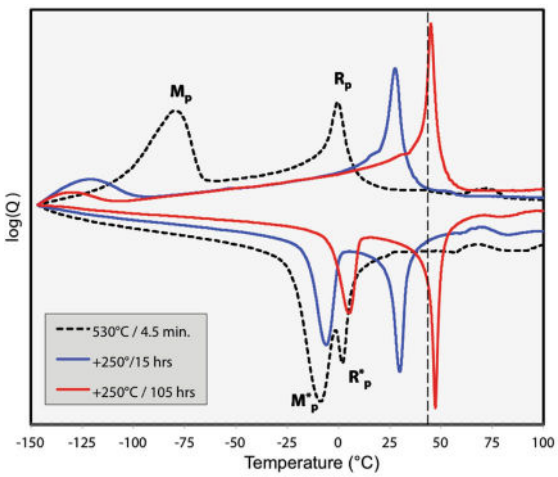

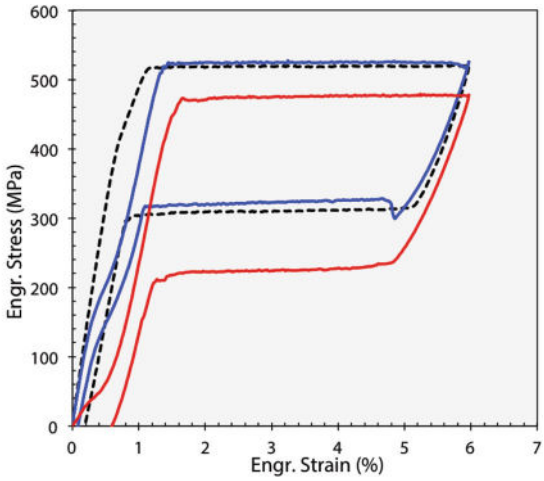

Fig. 1 DSC and 37 °C tensile curves of the same wire heat-treated three different ways are shown, highlighting that plateaus are not dependent upon Af. The dashed black curves represent a heat treatment that produces properties conventional to the medical device industry. The blue curve highlights that one can suppress Mp substantially without changing the upper plateau, and the red curve suppresses Mp further, yet shows a decrease in the plateau stress

and the resulting stress–temperature phase diagram will explain these trends. Indeed, we will see that superelasticity has nothing to do with the temperature range at which R reverts to A, but rather is dependent upon the temperature at which M reverts to R, denoted in Fig. 1 as M_p^*.

It is often helpful to draw an analogy between the stress–temperature phase diagram of Nitinol with the pressure–temperature diagram of water, with ice analogous to Martensite as the low entropy phase, and steam the high entropy phase analogous to Austenite. Upon cooling in a vacuum, ice forms directly from steam, but above a certain pressure (about 600 Pa) cooling produces a third phase of intermediate entropy, liquid. Theoreticians studying the phases of water on Mars would be oblivious to the existence of this intermediate liquid phase, and might struggle to understand why it is important to distinguish between the temperatures at which ice reverts and steam forms; synonymous in the vacuous atmosphere of Mars, the two are critically different at earth's atmospheric pressure.

While the basic thermodynamics governing the stability of the various phases at any given stress (pressure) and temperature are the same for Nitinol and water, there are a few differences. In the case of water, the volume difference between liquid and gas performs work and contributes to the stability of the competing phases. In Nitinol, the volume differences between all three competing phases are negligible, so to a first approximation, work production depends solely on the ability of the various phases to accommodate shape changes. The conventional phase diagram for water maps hydrostatic stress (pressure) against temperature whilst our Nitinol diagram will map deviatoric stresses (stresses that change the shape of the alloy rather its volume).

Be it water or Nitinol, at the phase boundary between any two phases (the *transus*), the Gibbs free energy of the two phases subjected to the same stress and temperature must be equal, giving us Eq. (1), simply stating that the work done as one forms a new phase must be offset by the release of chemical energy resulting from their entropy and internal energy differences.

$$\Delta H - T\Delta S - \sigma\Delta\varepsilon = 0. \tag{1}$$

Differentiating with respect to T leads to the familiar Clausius–Clapeyron equation:[1]

$$\mathrm{d}\sigma/\mathrm{d}T = -\Delta S/\Delta\varepsilon. \tag{2}$$

ΔS, the entropy difference between the two contending phases, is crystallographically determined, and to a first approximation, independent of temperature or microstructural detail. $\Delta\varepsilon$ is often viewed as the transformational strain, but rather it is the relative capacities of the competing phases to change shape under the applied stress and as such, a large component of which is the transformational strain. There will be further discussion regarding whether $\mathrm{d}\sigma/\mathrm{d}T$ is indeed crystallographically determined, but if one accepts that premise for the time being, determining the stress-free transformation temperatures defines the entire phase diagram, and the plateau stresses are known at any given temperature.

There are aspects of Nitinol's stress–temperature phase diagram that are simpler than that of water—for example, the liquid-steam transus is nonlinear because the volume of steam is dependent upon temperature. But in Nitinol, the

[1] While this is often written as $\mathrm{d}\sigma/\mathrm{dT} = -\Delta H/T\Delta\Delta\varepsilon$, care must be taken in that ΔH here is not the latent heat of transformation but includes strain energy considerations.

strain energy accumulates with transformation. There are several sources of strain energy associated with the transformation, including those attributed to the small volume change, interfacial stresses and dislocations. We can generally think of these in two categories, *conservative* and *non-conservative*. The former energy leads to a progressive type of transformation, meaning that the transformation requires an ever increasing driving force to proceed (e.g., super cooling to offset the accumulation of strain energy) and a distinct start and finish temperature. While these conservative energies are eventually returned to the system, non-conservative energies are frictional in nature and lead to a hysteresis—thus we need two diagrams, one for the *forward transformation* (the decomposition of Austenite toward phases of lesser entropy such as Martensite) and one for the *reverse transformation*, (transformation, or reversion, toward Austenite, the phase of greatest entropy).

Finally, in many circumstances, the behavior of Nitinol is often complicated by *strain localization*, or *Lüders bands* [3–5], which under certain circumstances can "cheat" thermodynamics of the strain energy discussed above, allowing the transformation to progress without increasing the driving force. This will be discussed in more detail below.

Several excellent reviews exist regarding the three competing phases [6–8], so we will keep our background discussion to a minimum. Like the B19' Martensite, the R-phase is a thermoelastic martensitic phase with variants that self-select to best accommodate the applied stress. While variant selection can produce strains in excess of 10% in the B19' Martensite (M), selection in the R-phase (R) only produces strains of 0.2–1.0%, depending upon the rhombohedral angle. Thus applied stresses stabilize both the R and M phase but R is stabilized to a much lesser extent. The kinetic obstacles to form R from A are much smaller than to form M directly, resulting in a much smaller hysteresis of 0–3 °C. Thus, even when M can be the more stable phase due to its lower entropy, R can still present until supercooling is able to overcome the formidable kinetic barriers to M formation. An additional attribute of the R-phase is that the structure of R is not fixed, but rather continues to change as it is stabilized: after initially forming in a first-order transformation to a rhombohedral angle of about 89°, the rhombohedral angle continues to contract (likely due to a second-order transformation) until the phase finally gives way to its successor, B19' Martensite.

While phase diagrams for Austenite, Martensite, and R-phase have often been schematically shown [9, 10], the objective here is to quantitatively determine the phase diagram using a variety of different test methods, and to do so on material that is typical of that used by the medical industry. In order to do this, it will be necessary to use more definitive terminology than that used by industry today. Specifically, we will use the usual "M" and "R" subscripted with "s," "f," and "p" to refer to the start, finish, and maximum activity (peak) temperatures for the formation of Martensite and R-phase upon cooling (collectively, the forward transformation), but will introduce the use of M^* and R^* (subscripted the same way) to signify the reversion of M and of R, regardless of the phase to which they revert. As examples,

R_s = the start of the transformation to the R-phase upon cooling (no change from the conventional ASTM F2005 terminology)

M_s = the start of the transformation to Martensite regardless of whether the parent phase is R-phase or Austenite (no change from the conventional terminology)

M_f^* = the completion of Martensite reversion regardless of whether it is reverting to R-phase or Austenite

R_p^* = the temperature at which the R-phase reverts most rapidly (typically halfway between R_s^* and R_f^*)

In this set of terminology, A_s and A_f retain their current meaning, but it is ambiguous which phase transforms to Austenite. In other words, A_f could mean R_f^* or M_f^* depending upon circumstances (by analogy, "formation of steam" does not differentiate sublimation from boiling).

Materials and Methods

The material used in this study is a typical superelastic wire used by the medical device industry, more specifically, it is 0.75-mm-diameter oxide-free wire from a 50.8 atomic percent alloy that was cold drawn 40%, then annealed at 550 °C with a stress and time at temperature sufficient to fully straighten the wire. The room temperature tensile properties of the wire are shown in Fig. 2. Just as with all tensile tests reported herein, each of the curves shown in Fig. 2 represents a sequence of independent tests on a virgin wire rather than the cycling of a single wire. All tensile testing was done in displacement control at an initial strain rate of 0.0003/s, consistent with ASTM standards [11], and all tests employed either a video or clip-on extensometer.

Thermal cycling under a constant load was done in an Instron operating in load-control. Loads were applied at 100 °C, the wires cooled to − 100 °C, then heated back to 100 °C (i.e., well below M_f and above A_f, respectively). Temperatures were controlled in an environmental chamber ramped at a rate of 4 °C/min.

Electrical resistance tests were also conducted in an Instron operating in load control, again by ramping temperature at a rate of 4 °C/min. A four-point method was used, passing a regulated 0.53 amperes through the wire

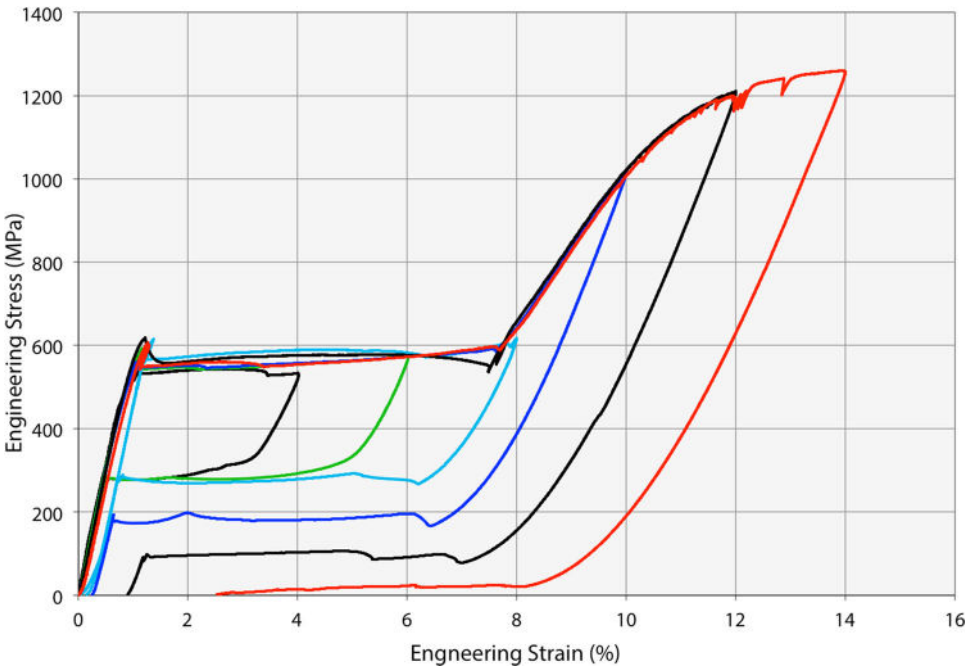

Fig. 2 Tensile curves of the wire used throughout this paper determined at room temperature show a Lüders yield drop and a flat plateau. As is typical, the unloading plateaus decrease with the introduction of plasticity. Each curve is a unique, untested wire. Not shown is the fracture itself, which generally occurred at 14–16% strain

and measuring the voltage drop between two points interior to the applied voltage. The distance between the measurement contacts was 8 cm. Stress-free tests were repeated in a highly dielectric liquid (Fluorinert FC770) and verified to be identical to the air experiments.

Differential Scanning Calorimetry was performed on a TA model Q100 DSC as prescribed by the ASTM F2005 standard for Nitinol [12].

The Forward Transformation

We begin by developing the phase diagram for the forward transformation: toward decreasing entropy, or from Austenite (A) toward Martensite (M). This will be examined in three steps: (1) identifying the formation of M (regardless of which phase is the immediate parent), (2) examining the formation of the R-phase (R) from A, and (3) combining the two curves to provide the full phase diagram.

Martensite Formation

The upper, or *loading plateaus* in the stress–strain curves such as shown in Fig. 2 provides our first method for locating the Martensite formation transus. Figure 3a shows individual loading profiles at a variety of temperatures. Plotting the plateau stresses then provides the $T-\sigma$ threshold for the formation of Martensite (Fig. 3b). While a slight inflection in initial loading hints that the parent is R at and below 0 °C, it is difficult to be certain so for now the phase diagram is labeled "Martensite" and "Parent" without specifically identifying whether the parent is A or R.

The plateaus in Fig. 3 appear at first to violate the thermodynamic principles discussed above. Specifically, it was pointed out that microstructural strain energy accumulates as the transformation to M proceeds, and for the transformation to progress, additional stress or supercooling is required (the DSC curves that will be shown below will demonstrate distinct start, peak, and finish to each transformation). Yet such flat plateaus are typical of the superelastic conditions used in medical devices, as is the stress drop that frequently occurs as one moves onto the deformation plateau. These features are due to the localization of strain into Lüders bands.

Localization of strain can be visualized by considering any buckling phenomenon, such as might be encountered when bending a thin-walled tubing: strain energy increases as the tube is bent until kinking occurs, abruptly localizing the strain and reducing the bending moment and the total strain energy of the system. When deformed in tension, Martensite first appears uniformly throughout the cross section, creating interfacial strain energy. As these strain fields impinge, the strain can localize at some heterogeneity and abruptly form bands that span the entire cross section. This locally reduces the cross-sectional area and increases the stress within the band, further stabilizing the banded Martensite. Martensite bands can then grow in width without increasing their interfacial area, so the strain energy is henceforth constant. This continues until the entire cross section is consumed and returns to a uniform

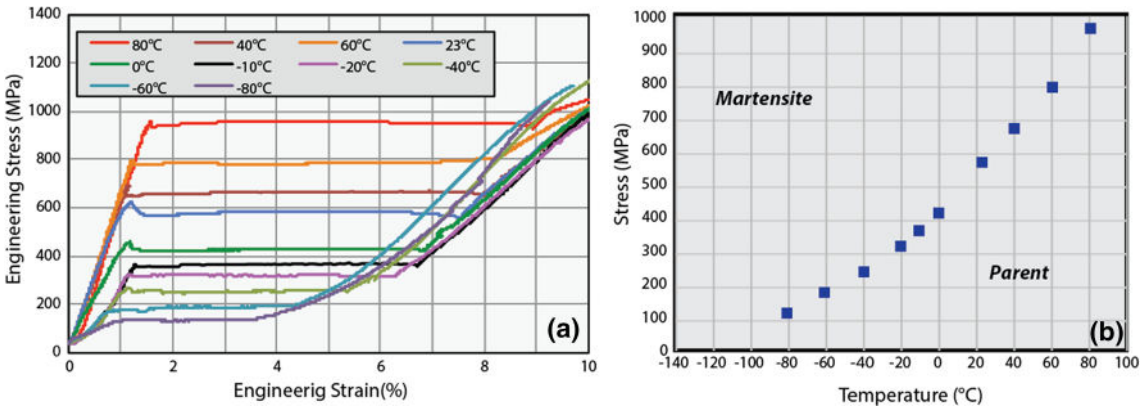

Fig. 3 Loading curves at various temperatures (**a**) show a monotonically rising forward transformation stress with temperature (**b**)

cross section. This strain localization is not observed in compression [3] or torsion [4], perhaps because strain localization does not result in a reduced cross-sectional area and local increase in stress. Moreover, the length of the plateau does not correspond to the transformational strain, but merely the stability range of the Lüders bands.[2] But for the purposes of constructing a stress–temperature phase diagram, there is just one stress to report—there is no separate "start," "peak," or "finish" stress for the transformation.

The Parent-Martensite transus of Fig. 3b was determined isothermally, but that transus should apply if one cools while maintaining a constant tensile stress (taking a horizontal rather than a vertical trajectory). The results of such experiments (cooling under various tensile stresses) are shown in Fig. 4. In addition to the primary tensile stretch, a small strain is observed in the − 20 °C to 0 °C range; this is due to the intervention of R, but for now, we remain focused on the transus for M formation regardless of whether A or R is the parent phase.

Examination of an electropolished wire surface during these tests showed distinct Lüders bands, so one might expect there to be no temperature interval between the start and finish temperatures, just as we saw no stress interval in the plateau stresses. Indeed, the small temperature intervals of Fig. 4 are artifacts of not having thermally quasi-static conditions: as the transformation proceeds, heat is produced which self-arrests the transformation. If one slows the cooling rate to 0.1 °C/min, giving time for the heat to dissipate, one indeed observes a step function response (see dashed line in Fig. 4). Thus, it is the M_s temperature that we expect to correlate to the plateau stresses of Fig. 3.

Figure 5 superimposes the constant-temperature and the constant-stress transus measurements. There appears to be a non-linearity, or perhaps two slopes to the Martensite transus, with a transition around at about 0 °C. To rationalize this, the R-phase must be introduced to our phase diagram.

R-Phase Formation

While the formation of R is evident in Figs. 3 and 4, determining the A–R transus is difficult using mechanical methods—the strains are small and diffuse, and the A–R transformation produces heat that can delay the transformation to M. Fortunately, the R-phase has a substantially greater electrical resistivity than either A or M, allowing one to track its progress with precision. Figure 6 shows the resistance of the wire during cooling under constant loads. The resistance is affected by both by resistivity changes as well as the geometry. As the wire is cooled, a sharp increase in resistance is observed as the R-phase is formed (annotated on the 300 MPa curve). While a small deformation contributes to the increase in resistance, the vast majority of the change results from the inherent higher resistivity of R. As the transformation to the R-phase completes, the change in resistance slows, but does not stop due to the continuously increasing R-phase distortion. With further cooling, the transformation to M itself begins. While M has a lower resistivity than R, resistance increases by $(1 + \varepsilon)^2$ due to the concomitant deformation. Again, we do not have quasi-static conditions with respect to calorimetric effects, so we should discount the M_p and M_f measurements.

As expected, the R-phase formation temperatures increase as stress is applied, but the rate of increase is substantially lower than that for M due to the smaller transformational strain of the A–R transformation. At

[2] Even in the absence of Lüders deformation, care must be taken in assuming that the plateau length is a measure of transformational strain. Neutron diffraction experiments have demonstrated that transformation continues well beyond the apparent end of the plateau [13]. Further evidence for this is seen in the temperature dependence of the plateau lengths in Fig. 3. It should be further noted that bands of Martensite do contain some small amount of retained Austenite, and some Martensite can still be found outside of the bands.

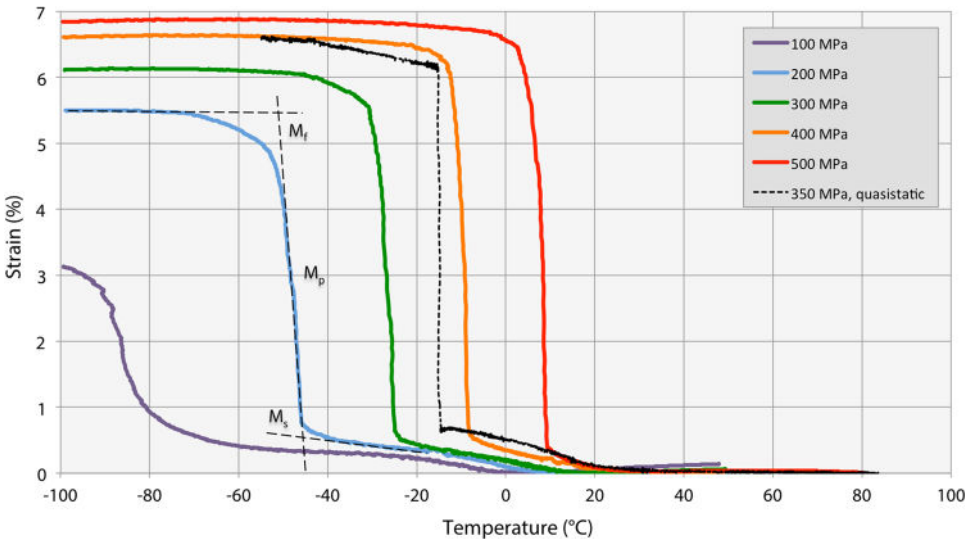

Fig. 4 Cooling under various constant tensile loads produces strains. The test indicated by the dashed black line was slowed to 0.1 °C/min, verifying that it is indeed M_s that should be correlated to the tensile plateaus

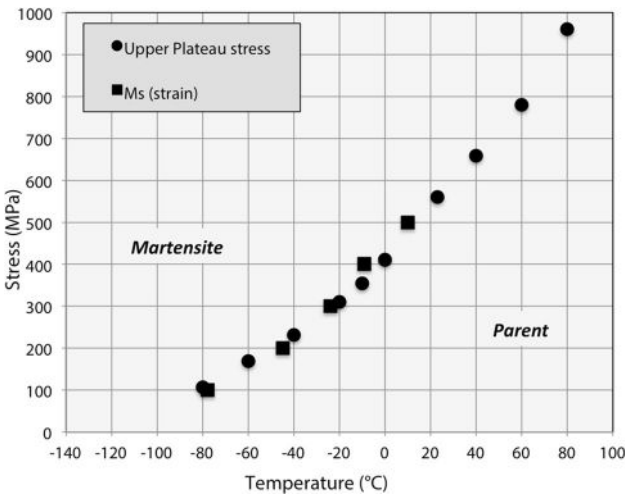

Fig. 5 Martensite formation transus by both tensile testing (circles) and measuring strain while cooling under constant loads (squares)

500 MPa, the R-phase is completely overrun by Martensite and there is no trace of an inflection—transformation to M is now direct.

The M_s temperatures from these tests are in excellent agreement with Fig. 5, but our primary interest is in using this tool to map R formation from A. Figure 7 shows both R_s and R_p determined by this resistance method, as well as a best-effort to extract the same data from Fig. 4. Peak temperatures were determined by differentiating the curves in Fig. 6 and locating the maximums. As discussed earlier, the rhombohedral angle of the R-phase continues to contract even after Austenite has been completely replaced, making R_f impossible to determine without diffraction methods.

All the data can now be combined to produce the full stress–temperature phase diagram for the forward direction (Fig. 8). In this figure, the color of each symbol indicates whether that specific test shows clear evidence of the nature of the transformation (direct A–M in blue, R–M in green, and A–R in red.) The triple point is about 485 MPa and 10 °C which means that the R-phase does not exist at either body or room temperature regardless of the applied stress.

Stress-Free Transformation Temperatures

The medical device industry often uses transformation temperatures as a control for plateau stresses; we assume that if one knows the transformation temperature, one can predict the plateau stresses. Maintaining the fore-mentioned assertion that the slopes of the three transformations of Fig. 8 are "crystallographically determined," the entire diagram is uniquely defined by the stress-free A–R and R–M transformation temperatures. (Again, we will discuss this assertion in the "Discussion" section below.)

Differential Scanning Calorimetry (DSC) is the only method to measure the forward transformation temperatures covered by an ASTM standard [12]. A DSC scan performed at the ASTM recommended scan rates is shown in Fig. 9. The cooling curve (in blue) corresponds to the forward transformation activity, an exothermic reaction. (The red reverse transformation peaks are included because they are important to the interpretation of the forward transformation.) The first peak encountered upon cooling (R_p) represents the heat released as R is formed from A, confirmed by the fact that the peak is mirrored during the heating cycle with very little hysteresis. The −14 °C peak temperature of the transformation of is in excellent agreement with the stress-free transformation on our phase diagram. Moreover, the A–R peak is in excellent agreement with the stress-free resistivity: Fig. 10 integrates the A–R (as well as the reverse R–A) DSC peaks and

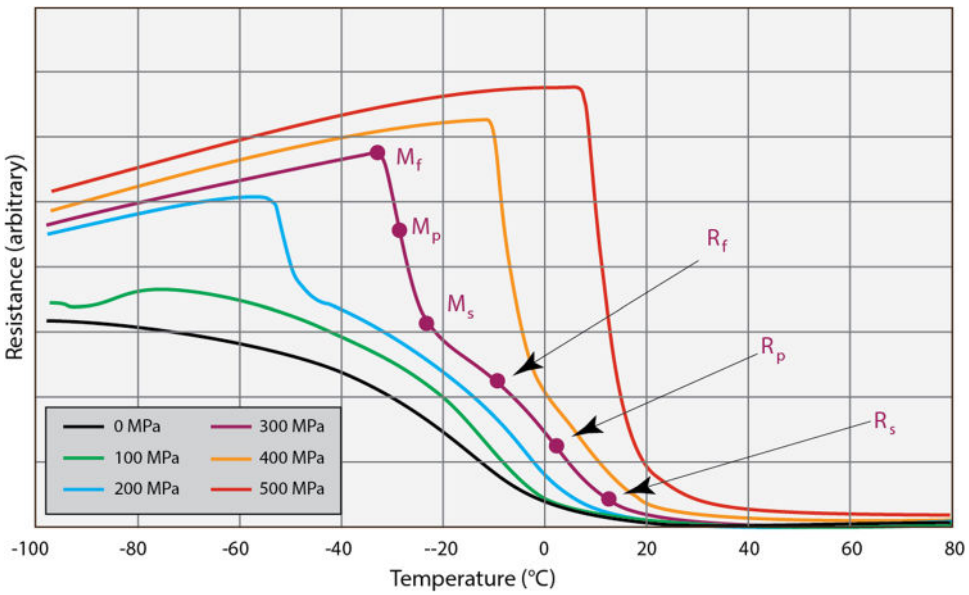

Fig. 6 The resistance of the test wire is measured during cooling under various loads. The 300 MPa curve is used to highlight the various transformation events that occur

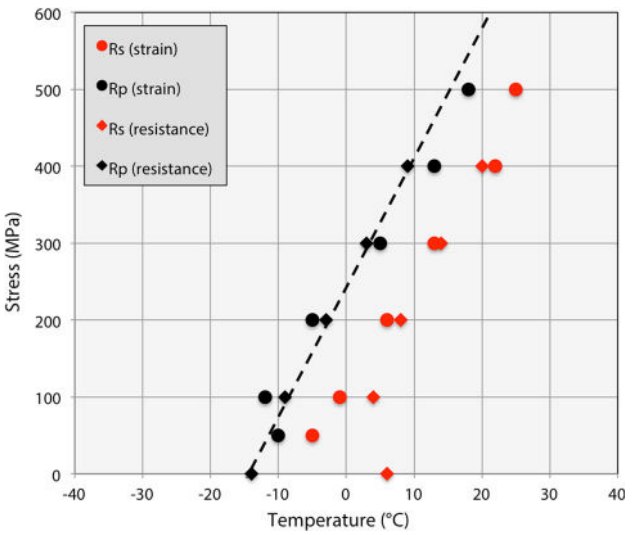

Fig. 7 R_s, R_p are mapped based on strain measurements from Fig. 4 (circles) and resistivity from Fig. 6 (diamonds). The stress rate for the transformation was determined to be 17.0 MP/ °C. Calculation of the slope is based on resistance values only

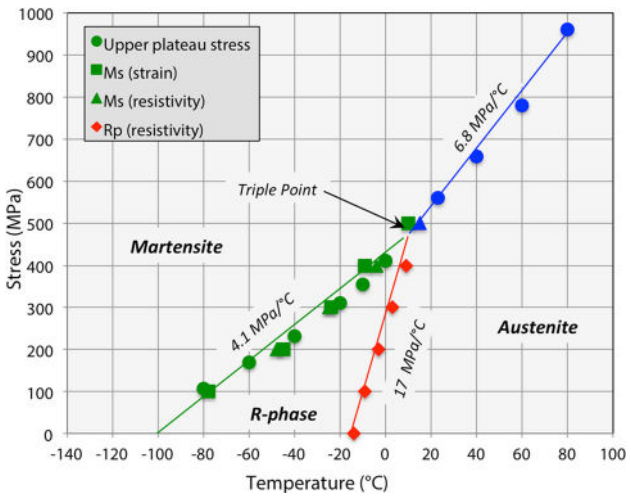

Fig. 8 The phase diagram for the forward transformation (toward decreasing entropy, or from lower right to upper left). The symbol shapes indicate the measurement technique, and the color the transformation: A-M (blue), A-R(red), and R-M (green)

normalizes them with the resistance curves. The agreement between methods is excellent.

The second peak encountered during cooling is more difficult. While there is a disturbance in the DSC trace at about − 100 °C, it is unclear whether it is a real signal or baseline drift. Such low-temperature peaks are normally weak and diffuse; however, one can still accurately map the R-to-M transformation by beginning the heating cycle at various temperatures and examining the progress of the reverse transformation peak (M^*); the volume fraction of M reverted must be the volume fraction that was formed in the first place. This is done in Fig. 11, showing an M_s temperature of − 103 °C and an M_p of − 125 °C, in agreement with Fig. 8.

While DSC is an insightful and accurate tool, it can be easily misread: if this wire had only been cycled to − 80 °C, one would have observed one cooling peak and one heating peak, neither of which would have anything to do with M nor the performance of the material.

The Reverse Transformation Phase Diagram

The reverse transformation is often the more important. It reflects, for example, the stress applied by a device against a vessel wall after being released from a catheter. It thus

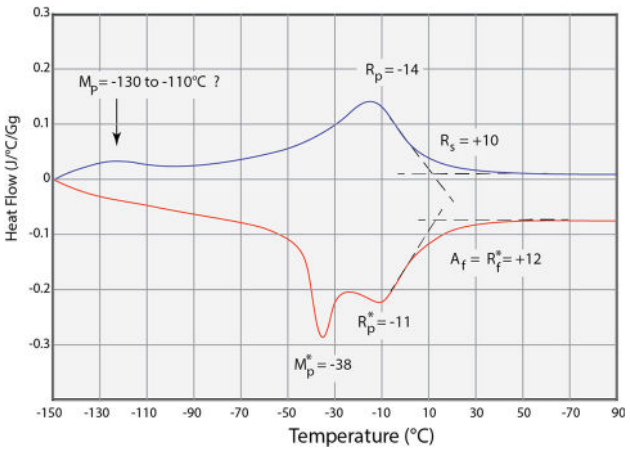

Fig. 9 DSC trace for the subject wire shows two clear peaks during the reverse transformation, but only one clear peak and one possible peak upon cooling. Yet we know there must be two transformations upon cooling since obviously one cannot revert Martensite without first forming Martensite

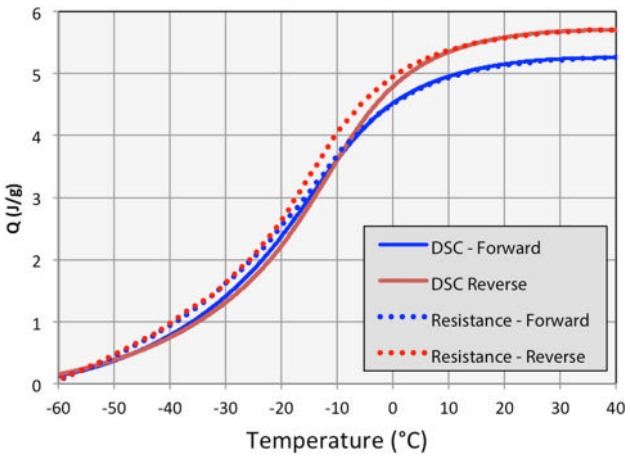

Fig. 10 The forward A-R and reverse R-A DSC peaks are isolated by restricting cooling to − 80 °C to prevent Martensite formation, then integrated in both the forward and reverse directions and compared with the stress-free resistance measurements (resistance has been normalized to the total heat flow.)

defines the equilibrium lumen diameter. While measuring the reverse transformation temperatures is more straightforward from an experimental perspective, interpretation can be more difficult, largely because the role of the R-phase is more subtle and easier to overlook. During reversion, the R-phase does not benefit from the large hysteresis of the M-to-R transformation—in fact, the R-phase is sometimes completely absent from the reversion process, and in these cases M_f^* is synonymous with A_f. In the wire tested here, as in most thermomechanically treated medical devices, the R-phase makes an appearance during heating, but it is subtle.

As seen in Fig. 2, plastic deformation reduces the unloading plateau. To avoid this, a 6% deformation was chosen (Fig. 12). While this avoids plasticity, the transformation to Martensite is now incomplete, so the stress drop observed upon loading is not mirrored during unloading. Note in Fig. 2 that higher deformation strains that do "complete" the transformation exhibit a reverse stress drop at the beginning of the unloading plateau. So while the plateaus are not perfectly flat, we can still be reasonably accurate by taking the stress at the midpoint of recovery.[3]

Figure 13 examines the recovery strain during heating under fixed tensile loads following the deformations of Fig. 4, and Fig. 14 shows resistance measurements during heating under various fixed stresses. Since cooling with 10 and 100 MPa stresses is insufficient to cause comparable deformation, these two load conditions were prestrained to 6% at − 100 °C prior to applying the 10 and 100 MPa loads. As before, when the tests are slowed sufficiently to achieve quasi-static conditions, a step function recovery is observed (dashed line in Fig. 13), so again, thermal recovery profiles experience thermal arrest.

Figure 15 summarizes the data from tensile, constant stress–strain measurements, and constant stress resistance. The R-phase, while present, has a more limited scope during heating because it no longer benefits from the kinetic barriers to Martensite formation, so there are less data available to define the A–R and M–R boundaries and the $d\sigma/dT$ estimates are more difficult.

DSC and BFR Testing

There are two ASTM-governed methods for measuring the stress-free reversion transformation temperatures: DSC [12] and Bend Free Recovery (BFR) [14]. We begin with DSC (Fig. 9). The Martensite reversion peak ($M_p^* = -37$ °C) agrees well with the phase diagram of Fig. 14. Reversion of R-phase ($R_p^* = -12$ °C) agrees reasonable well, though again, it is difficult to pin down the phase boundary with such limited data. Note that, the M^* and R^* peaks can be deconvoluted by running a second DSC cycle down to − 80 °C—this removes the M^* peak and isolates the R^* peak, which can be subtracted from the full cycle to isolate the M–R peak. This method is extremely effective in separating even the slightest of shoulders on the main reversion peak.

Bend Free Recovery was run in accordance with ASTM F2082-06, with no measurable load (Fig. 16). The test was

[3] Not that, this midpoint stress value could be different from the unloading stress values dictated by ASTM F2516. Here, we are invoking thermodynamic principles, whereas the ASTM standard provides a convenient, yet arbitrary, strain (2.5%) to select an unloading stress..

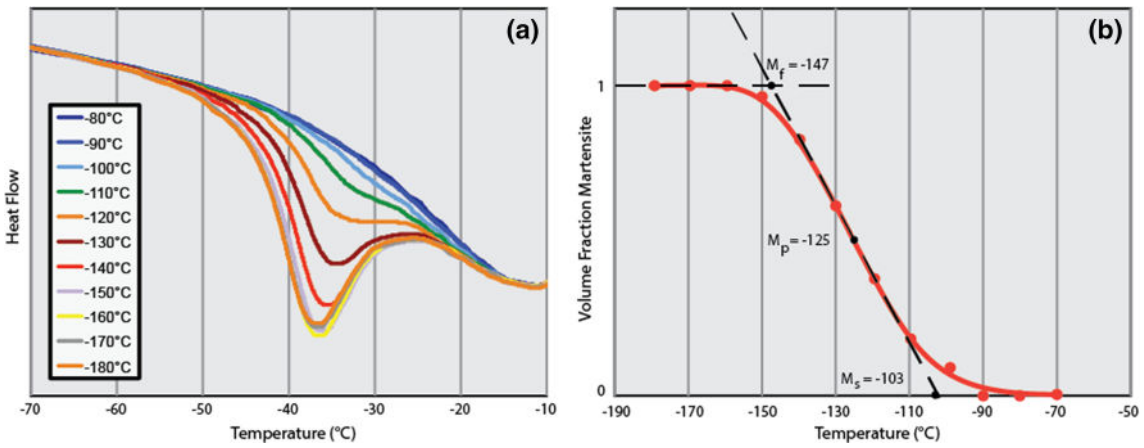

Fig. 11 **a** shows how the heat associated with the M* peak increases as the wire is cooled to increasingly low temperatures (− 80 °C to − 180 °C). Integrating the peaks of (**a**) provides Ms, Mp, and Mf (**b**)

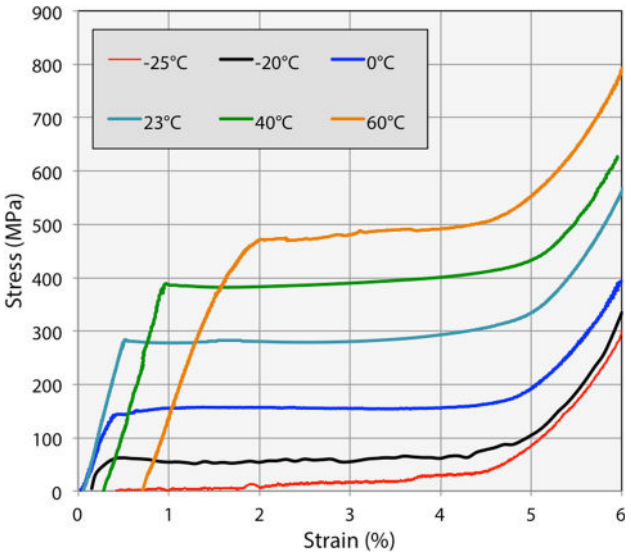

Fig. 12 Unloading traces after 6% deformations. Unloading plateau stresses are defined as the inflection point during unloading

found to be very reproducible but there are several reasons to expect a poor correlation to the tensile plateaus:

- The ASTM method for BFR specifies that the maximum strain imparted to the samples should be limited to 2–3% in order to avoid the fore-mentioned effects of plastic deformation. With an outer fiber strain of 2%, the actual volume fraction of Martensite in the entire cross section is less than 5%. This typically results in an upward shift in M_s^* and M_p^* with respect to the reversion of a fully Martensitic sample.
- According to ASTM, the deformation temperature is − 55 °C, at which the wire is in the R-phase; therefore, the Martensite is stress induced for these wires.
- Bending produces both compression and tension. Compression has a smaller transformational strain and consequently, a larger $d\sigma/dT$—the transus for a compressive phase diagram looks entirely different, with steeper A–M and R–M slopes.
- Because there is a strain gradient through the wire cross section, there are elastic residual stresses accumulated during the forward transformation that assist reversion.
- The phase diagram created for tension assumes Lüders strain localization. If Lüders bands are present in a BFR test, they will be superficial and only on the convex side of the bend, so strain energy barriers to transformation should be expected to be greater.

Excepting the first two points, one can resolve the above by performing the experiment in tension rather than bending (green trace in Fig. 16). Here, a wire is deformed 2% in tension at − 100 °C, then heated to examine shape recovery. The agreement of M^* measured in tension and DSC is excellent.[4] Although a clear R-to-A transformation is observed in tensile recovery, it occurs at a temperature substantially lower than indicated by DSC or resistivity. As pointed out, however, strain is an insensitive and inaccurate method of detecting the R-phase.

The Effect of Plastic Deformation on the Reverse Transformation

As shown in Fig. 2, unloading stress plateaus decrease with increasing deformation strain. Increasing deformation strain leads to plasticity with in turn stabilizes Martensite both due to residual stress fields and due to Martensite

[4] Extracting the M_s^* temperature is difficult because shape recovery is so gradual. One must project the recovery profile to estimate the horizontal tangent, as shown in this figure. The alternative of drawing a tangent to the tail of recovery is even more problematic since then the temperature at which one begins to record data dictates the slope of the tangent.

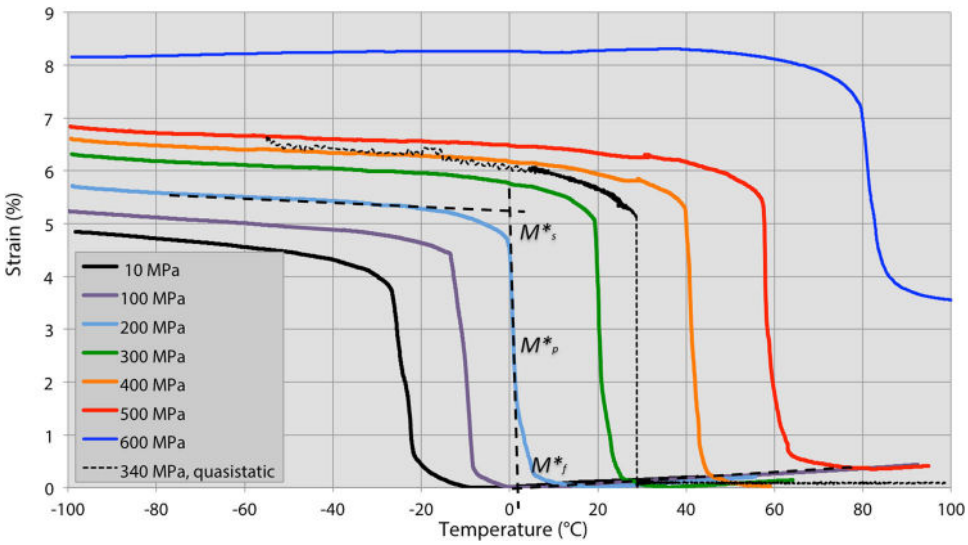

Fig. 13 Heating with various tensile loads applied. The initial deformations are shown in Fig. 4, with the exception of the 10 MPa and 100 MPa curves which were prestrained to 6% strain prior to testing

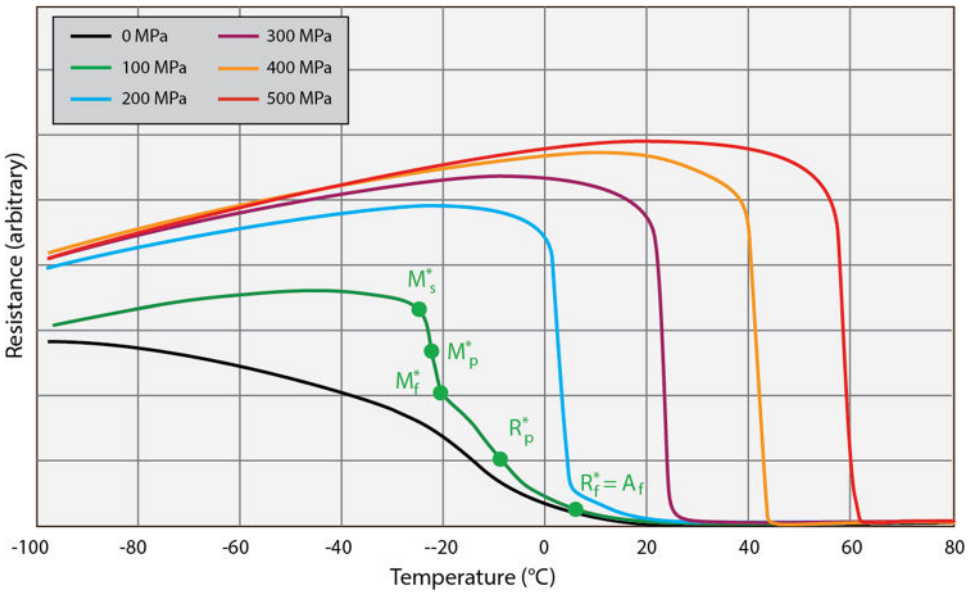

Fig. 14 Resistance during heating, after the cooling shown in Fig. 6

plates binding to dislocations. The reverse transformation phase diagram is therefore not a material property, but is history dependent. To provide some insight into this dependence, the unloading plateaus were measured after various deformations, producing Fig. 17. This pinning is temporary in the sense that full reversion, either by heating or unloading, will return the plateau to its original state (Fig. 18).

Discussion

Figure 19a summarizes the forward transformation phase diagram, removing the individual data points for the sake of clarity, and describes what might be called an *effective* $d\sigma/dT$ for Martensitic formation, which is a weighted average of the A–M and R–M boundaries, leveraged about the triple point, T_t:

$$(d\sigma/dT)_{\text{effective}} = \left[(d\sigma/dT)_{A-M}(T_A - T_t) + (d\sigma/dT)_{R-M}(T_t - M_s)\right]/(T_A - M_s) \quad (3)$$

where T_A indicates ambient temperature. Continuing to use the forward transformation as a model, we now examine at three heat treatment scenarios:

- Figure 19b treats the case where both M_s and R_s are both decreased by 25 °C. While indeed the upper plateau stress moves upward as shown, that boost benefits from an increase in the effective $d\sigma/dT$, brought about by the lowering of the triple point.
- Figure 19c treats perhaps a more common case, in which Martensite is suppressed by 25 °C, but the

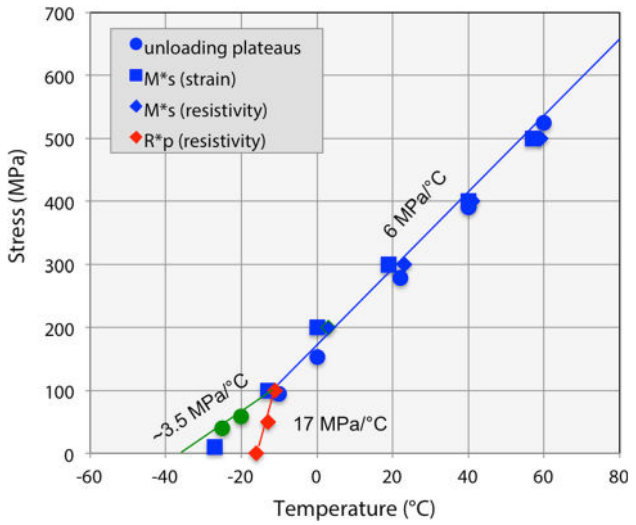

Fig. 15 The reverse transformation phase diagram comprising data from tensile testing, constant stress thermal cycling, and resistance measurements

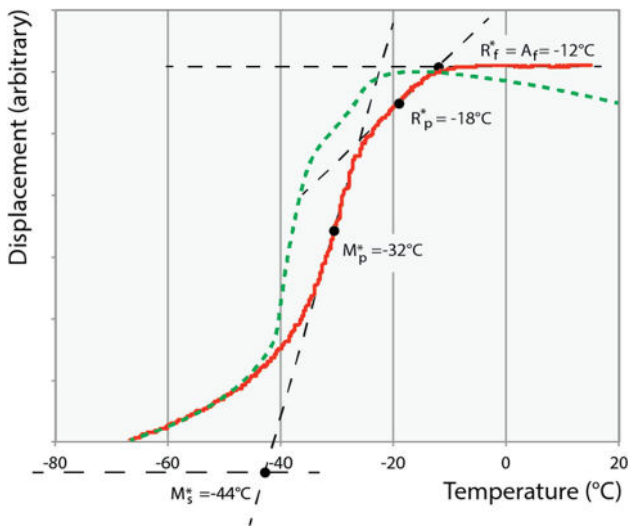

Fig. 16 Bend Free Recovery after a 2% deformation (red) is normalized and superimposed with a stress-free tensile free recovery after a 2% tensile deformation (green)

R-phase is unchanged. In this case, there is only a small increase in plateau stress due to decrease in the effective $d\sigma/dT$.

- Figure 19d treats the case in which Martensite is suppressed by 25 °C and R_s is increased by 25 °C. The triple point is now moved sharply upwards and the effective $d\sigma/dT$ is lowered so much that the upper plateau stress remains unchanged. Moreover, because the triple point is now above ambient temperature, the R-phase appears during loading.

The above highlights the treacherous nature of the R-phase. Body temperature superelastic cycling of the

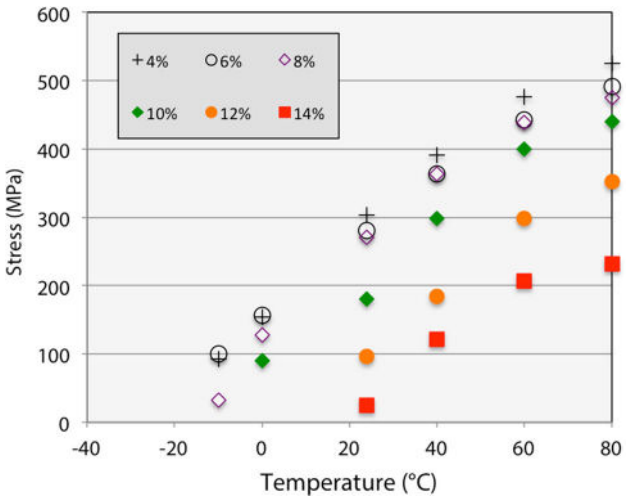

Fig. 17 Unloading plateaus are shown as a function of temperature and total strain, demonstrating that at all temperatures, strains above 8% stabilize Martensite and lower plateau stresses

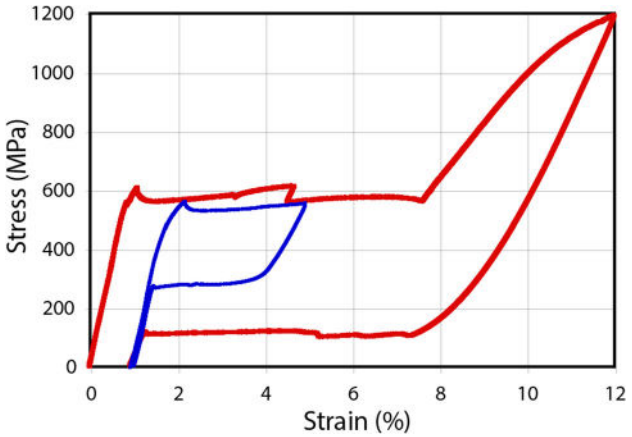

Fig. 18 The stabilization of Martensite with plastic deformation manifests as a decreased unloading plateau. Upon full reversion, either through heating or unloading, stabilization effects are lost and the unloading plateau reverts to its original level (blue curve)

alloys of Figs. 19a, 19b, and 19c does not cause the appearance of the R-phase, so one might be lulled into ignoring it. Yet it plays a critical role in controlling the plateau stress due to its effect on $(d\sigma/dT)_{effective}$. With this construction in place, we now revisit Fig. 1. The red curve shows a 60 °C suppression of Martensite formation from the unaged dashed curve, yet the upper plateau stress is reduced—it is substantially more difficult to thermally induce Martensite but easier to stress induce Martensite. Of course the same construction and logic holds for the reverse transformation.

There remains much to be learned about how the R and M peaks can be moved independently and how the triple point can be manipulated. Precipitation enriches the matrix in titanium which boosts transformation temperatures, but

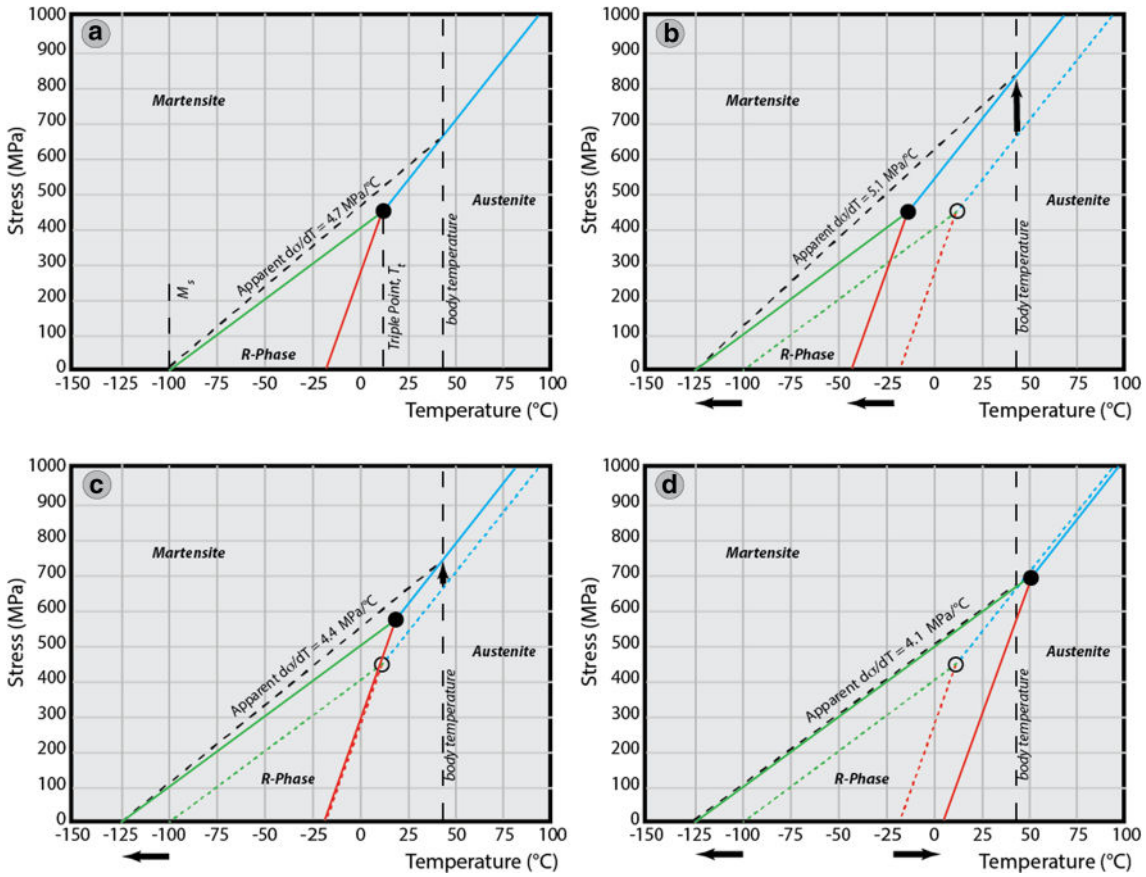

Fig. 19 **a** shows the concept of an effective dσ/dT, leveraged about the triple point, Tt. **b**, **c**, and **d** show four heat treatment scenarios, the arrows on the temperature axis denoting the movement of the transformation temperatures, and the resulting increase in the loading plateau indicated by the arrow at body temperature

precipitation also distorts the lattice and creates microstructural stress inhomogeneities which impede transformation. Martensite, with a far greater $\Delta\varepsilon$, is more strongly influenced by the stress inhomogeneities than is the R-phase. This suggests that coherent precipitation should separate the M and R transitions, consistent with the observations herein. When further aging leads to a loss of coherency, the influence of stress inhomogeneities is lessened, and we observe a chemical stabilization of both M and R.

We now turn to the contention that the phase boundary slopes are crystallographically determined. As shown in Eq. (2), the slope of each transus is equal to the entropy difference between the two phases (ΔS) divided by the ability of each phase to do work (to change shape ($\Delta\varepsilon$) in response to the applied stress). Both factors will now be discussed in turn.

To a first approximation, ΔS_{A-M} and ΔS_{A-R} should indeed be crystallographically determined, ignoring possible contributions from vibrational entropy and defects [15, 16]. The R-phase, however, is not a fixed structure, but continues to decrease its rhombohedral angle with cooling. ΔS_{R-M} should therefore decrease as the R-phase is cooled, potentially leading to non-linearity in the R–M boundary. But since the R-phase transformational strain increases with cooling, $\Delta\varepsilon_{R-M}$ decreases. With both numerator and denominator decreasing, is unclear what should happen to the Clausius–Clapeyron ratio, but the present data suggest that it remains largely constant.

More influential is the variability in the ability of Martensite to accommodate stresses, leading to variability in $\Delta\varepsilon_{A-M}$ and $\Delta\varepsilon_{R-M}$. Firstly, we wish to emphasize that $\Delta\varepsilon$ is not the transformational strain, but rather the total strain response of the two contending phases to a given stress. For example, annealed aluminum would be able to shed strain energy more readily than hardened steel, not because of a phase transformation, but because aluminum exhibits a lower elastic modulus and plastically deforms more easily. It is not important how a phase reduces strain energy, rather simply that it does so. Having said that, in the case of

Martensite, a dominant part of $\Delta\varepsilon$ is the transformational strain. Accordingly, we must be aware that the phase diagrams derived here are only valid for tension. The $d\sigma/dT$ for Martensite formation and reversion would be much steeper for compression, due to the lower transformational strain. For the same reason, the orientation of the testing direction to the crystallographic texture plays an important role: the largest $\Delta\varepsilon$ is found near the $\langle\ 1\ 1\ 1\ \rangle_A$ direction [17] which is close to observed wire drawing textures.

To exemplify some of these points:

- The concave side of a wire bent above M_p^* will have a higher $d\sigma/dT$ than the convex, or tensile, side. It will, therefore, have higher plateau stresses, and the magnitude of the difference between the two sides will increase with temperature.
- A textured wire will have a higher $\Delta\varepsilon$ and therefore $d\sigma/dT$ than a fully annealed wire or other form.
- The long transverse direction of flattened wire and sheet will produce higher stresses but accommodate less strain than would the longitudinal direction.
- The plateau stresses of stent struts cut from tubing will vary depending upon the direction of their directionality within the plane of the tubing (axial versus circumferential directions).

The total heat flow of each of the DSC peaks also warrants discussion. For hysteresis-free transformations such as those in water, the heat absorbed or released (Q) is the difference in enthalpy between the phases. In Nitinol, however, there are non-conservative contributions to Q. These dissipative energies are likely large for Martensite formation and reversion, but small in the case of the nearly hysteresis-free A–R transformation. Thus, one might expect the DSC to provide a reasonably accurate ΔH value that might, in turn, be used to calculate $(d\sigma/dT)_{A-R}$. Figure 10 shows the forward and reverse A–R transformational activities in isolation, determined by cooling only to − 80 °C so as to completely avoid M formation and integrated to show transformational progress, and total heat flow, Q. (The endothermic reverse peak has been flipped to facilitate comparison, and the zero-stress resistivity curves are superimposed in order to test consistency.)

Figure 10 verifies that the A-R transformation is indeed almost hysteresis free, with the DSC showing a 2 °C hysteresis and the resistivity essentially no hysteresis. Yet $Q_{forward}$ and $Q_{reverse}$ differ by approximately 10%, indicating that there are still non-conservative contributions to Q. Even in this case, the DSC is unable to directly predict $d\sigma/dT$. If one takes the average of the forward and reverse heat flows to be ΔH and one assumes a $\Delta\varepsilon$ of 0.5%, one would predict a $\Delta\varepsilon_{R-A}$ of approximately 35 MPa/ °C.

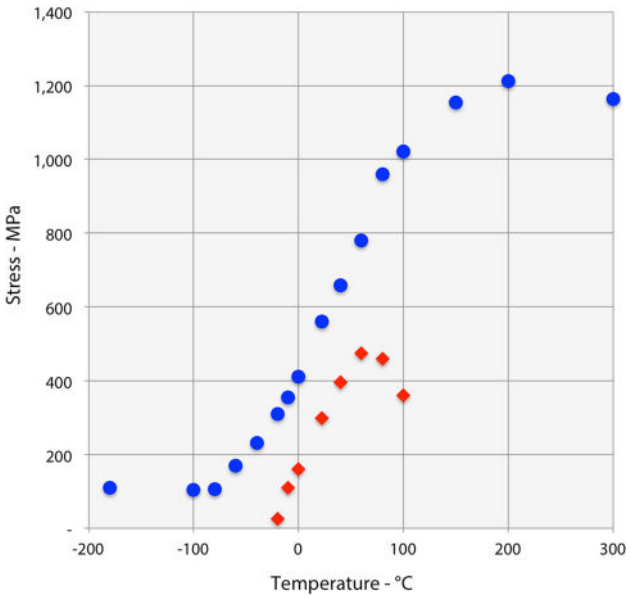

Fig. 20 Extending the tensile testing regime beyond the well-behaved Clausius–Clapeyron regime, with low temperature yielding controlled by twinning stresses, and plasticity playing an increasingly important role at high temperatures. The stresses reported here are 1% offset yield stresses

Behavior Outside the Clausius–Clapeyron Regime

While perhaps tangential to the primary interests of this paper, for the sake of completeness, we extend the temperature range beyond that governed by the Clausius–Clapeyron equation (Fig. 20). Below M_s, the upper plateau is controlled by the Peierls stresses associated with twin boundary movement. At high temperatures, plastic deformation begins to compete with transformation, ultimately arriving at the M_d, or *Martensite Desist,* temperature. M_d is the temperature at which plastic deformation comes at a lower energetic price than maintaining the low entropy Martensite phase—either Austenite itself deforms, or Martensite forms but immediately plastically deforms, lowering the stress and reverting to Austenite. Either way, Martensite can no longer be tolerated regardless of the stress. As shown in Fig. 20, M_d is more of a concept than a measureable temperature—there is a wide range of temperatures over which deformation is shared between plasticity and transformation.

Conclusion

A stress–temperature phase diagram has been constructed for a cold worked and aged wire typical of those used by the medical device industry. It was shown that when Lüders bands are present, plateau stresses can be predicted based on the start temperatures for the forward and reverse

transformations, M_s and M_s^*. To do so, however, requires one to construct an effective Clausius–Clapeyron ratio that hinges upon the triple point of the phase diagram. By moving the triple point to higher temperatures, one can reduce the transformation temperatures to and from Martensite, and actually reduce the plateau stresses. Put another way, one can make it more difficult to thermally induce Martensite, yet easier to stress induce Martensite. It was also shown that one can achieve superelasticity even when the A_f temperature is above ambient temperature. Perhaps most importantly, a new set of terminology has been proposed that avoids the ambiguity of whether the R-phase or Austenite is the parent phase to Martensite.

References

1. Duerig TW, Bhattacharya K (2015) The influence of the R-phase on the superelastic behavior of NiTi. Shap Mem Superelasticity 1:153–161
2. A Shamimi, B Amin-Ahmadi, A Stebner and TW Duerig, The Effect of low temperature aging and the evolution of R-phase in Ni-rich Ni-Ti, to be published
3. Reedlunn B, Churchill CB, Nelson EE, Shaw JA, Dally SH (2012) Tension, Compression, and Bending of Superelastic Shape Memory Alloy Tubes. J Mech Phys Solids 63:506–537
4. McNaney JM, Imbeni V, Jung Y, Papadopoulos P, Ritchie RO (2003) An experimental study of the superelastic effect in a shape-memory nitinol alloy under biaxial loading. Mech Mater 35:969
5. Sun QP, Li Z-Q (2002) Phase transformation in superelastic NiTi polycrystalline micro-tubes under tension and torsion—from localization to homogeneous deformation. Inter J Solids Struct 39(13):3797
6. Otsuka K, Ren X (1999) Physical metallurgy of ti-ni-based shape memory alloys. Intermetallics 7:511
7. Ling HC, Kaplow R (1981) Stress-induced shape changes and shape memory in the R and martensite transformations in equiatomic NiTi. Met Trans 12A:2101
8. Miyazaki S, Otsuka K (1986) Deformation and Transformation Behavior Associated with the R-phase in Ti-Ni Alloys. Met Trans A 17:53–63
9. Wang X, Kustov S, Verlinden B, Van Humbeeck J (2015) Fundamental Development on Utilizing the R-phase Transformation in NiTi Shape Memory Alloys. Shap Mem Superelasticity 1(2):231
10. Helbert G, Saint-Sulpice L, Chirani SA, Dieng L, Lecompte T, Calloch S, Pilvin P (2017) A uniaxial constitutive model for superelastic NiTi SMA including R-phase and martensite transformations and thermal effects. Smart Mater Struct 26:1
11. ASTM Designation: E6—09b, Standard Terminology Relating to Methods of Mechanical Testing
12. ASTM Designation: F 2004—05, Standard Test Method for Transformation Temperature of Nickel-Titanium Alloys by Thermal Analysis
13. Stebner AP, Paranjape HM, Clausen B, Brinson LC, Pelton AR (2015) In situ neutron diffraction studies of large monotonic deformations of superelastic nitinol. Shap Mem Superelasticity 1:252–267
14. ASTM Designation: F 2082—06, Standard Test Method for Determination of Transformation Temperature of Nickel-Titanium Shape Memory Alloys by Bend and Free Recovery
15. Bogdanoff PD, Fultz B (2001) The role of phonons in the thermodynamics of the martensitic transformation in NiTi. Philos Trans B 81:299
16. Stebner AP, Vogel SC, Noebe RD, Sisneros TA, Clausen B, Brown DW, Garg A, Brinson LC (2013) Micromechanical quantification of elastic, twinning, and slip strain partitioning exhibited by polycrystalline, monoclinic nickel-titanium during large uniaxial deformations measured via in situ neutron diffraction. J Mech Phys Solids 61(11):2302–2330
17. Cai S, Schaffer JE, Ren Y, Yu C (2013) Texture evolution during nitinol martensite detwinning and phase transformation. Appl Phys Lett 103:241909